

# Coherent optical computing for T-ray imaging

Kanghee Lee,<sup>1</sup> Kyung Hwan Jin,<sup>2</sup> Jong Chul Ye,<sup>2</sup> and Jaewook Ahn<sup>1,\*</sup>

<sup>1</sup>Department of Physics, Korean Advanced Institute of Science and Technology, Daejeon 305-701, Korea

<sup>2</sup>Department of Bio and Brain Engineering, Korean Advanced Institute of Science and Technology, Daejeon 305-701, Korea

\*Corresponding author: [jwahn@kaist.ac.kr](mailto:jwahn@kaist.ac.kr)

Received September 30, 2009; revised December 9, 2009; accepted January 11, 2010;  
posted January 15, 2010 (Doc. ID 117850); published February 8, 2010

Single-point imagery of 2D objects is proposed by exploiting the extreme broadband nature of an ultrafast terahertz wave. In the proposed imagery, a collimated terahertz beam is illuminated on an object, and the scattered fields are measured through a hole at the Fourier plane in a conventional terahertz time-domain spectroscope. This arrangement allows conversion of radial spatial frequencies of the object to the temporal spectrum of the pulse. Hence, a 2D image can be readily obtained by rotating a hole around the optical axis. Experimental results confirm that a complicated object can be reliably imaged using only 30 waveform measurements. © 2010 Optical Society of America  
OCIS codes: 110.6795, 320.7100.

Coherent optical computing deals with acquisition and manipulation of information carried by electromagnetic or acoustic waves and has found many applications in image and signal processing [1,2]. The basic operation is the double-Fourier transformations of an object  $U(x,y)$ , to form an image  $V(x',y')$ , in an optical system, for example, consisting of transform and image lenses and a Fourier domain filter  $M(k_x,k_y)$ , i.e.,

$$V(x',y') = \mathcal{F}^{-1}[M(k_x,k_y) * \mathcal{F}\{U(x,y)\}], \quad (1)$$

where  $\mathcal{F}$  is the Fourier transform and  $*$  is the convolution integral. This well-known relation between the object and image in a given optical computing system is defined for a monochromatic scalar wave. However, by using an extreme broadband nature of ultrafast terahertz (THz) wave [3], a different kind of computing, for example, encryption of the object function  $U(x,y)$  into a temporal waveform  $V(t)$ , may be possible. In this Letter, we report an application of coherent optical computing, namely single-point imagery, whereby a broadband coherent wave is used to encrypt and decrypt 2D images.

In a conventional theory of Abbe for image formation [2], the spatial frequency components of an object are measured by scanning the detector across the diffracted beams in the Fourier plane, as shown in Fig. 1(a). However, for an extremely broadband source, a single detector placed in a fixed position, as shown in Fig. 1(b), measures the broadband THz frequencies that have one-to-one correspondence with the spatial frequencies of the object. The ultrafast THz wave is an electromagnetic pulsed source of terahertz carrier frequency and of extremely broad bandwidth up to  $\delta\omega \approx 20$  THz [3]. Among the currently available ultrafast EM sources, it is the only source with the frequency-to-bandwidth ratio of near unity, i.e.,  $\delta\omega/\omega \approx 1$ .

The characteristic of extreme frequency-to-bandwidth ratio and the short-pulsed nature of THz wave have been already playing an essential role in the past development of THz imaging methodologies

[4–8]. Most of the conventional THz imaging techniques are based on the THz time-domain spectroscopy (THz-TDS) [9] performing a simple raster scan with mechanical delays, so the acquisition speed is one of the limiting factor in real applications. To overcome this, 2D electro-optic imaging [10], THz detectors array [11], and reciprocal imaging technique [12] have been proposed at the cost of high implementation complexity. Recently, Chan *et al.* [8] have employed a compressed sensing technique [13] for THz imaging. Here, using only a single detection and intelligent choices of spatial modulation, they reduced the image acquisition time significantly. However, this work was mainly based on THz-intensity measurement rather than exploiting the extremely broadband nature of the THz spectrum. It is now well known that the broadband THz signal can be reliably measured using THz-TDS. Furthermore, fast waveform measurement is under active investigation, for which mechanical scanning is now being replaced by electro-optical scanning skill as phase-locked THz-asynchronous optical sampling (AOS) [14,15]. Here, we exploit the extremely broad bandwidth of THz signal to drastically reduce the number of samples, hence, to accelerate the acquisition time.

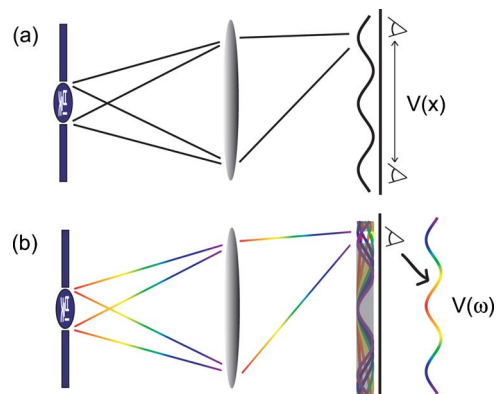


Fig. 1. (Color online) Concepts of (a) conventional usage of monochromatic wave for image formation and (b) single-point imagery using extreme broadband source.

In the proposed single-point THz imagery, the target object is placed in the object plane  $\Sigma_o(x,y)$ , as shown in Fig. 2(a), and illuminated by a collimated THz wave. The diffracted field from the object  $U(x,y)$  is then collected by a transform optic and is propagated to the Fourier plane  $\Sigma_t(\xi,\eta)$ , where the spatial frequency vector is  $(k_x, k_y) = (k\xi/f, k\eta/f)$ . Here,  $f$  is the focal length of the transform optic and  $k = \omega/c$  is the wavenumber of the incident wave. Now a Fourier filter  $M(\xi,\eta)$  is placed as shown in Fig. 2(b). Then, even a specific spatial frequency  $\vec{k}$  is sampled, owing to the broad bandwidth of wave, the whole range of  $\delta\vec{k} = \delta\omega/c(\xi/f, \eta/f)$  is still measured by a detector placed at the center of the image plane  $\Sigma_i(x',y')$ .

This idea is explained using Fourier optic theory [2]. As  $M(\xi,\eta)$  is located at the far field, the THz field spectrum  $V(\omega)$  measured at the detector is

$$V(\omega) = C(\omega) \int_{\Sigma_t} d\xi d\eta \int_{\Sigma_o} dx dy \times [M(\xi,\eta)U(x,y)e^{-ik(x\xi+y\eta)/f}], \quad (2)$$

where  $C(\omega) = S(\omega)(\omega/2i\pi f)^2$  and  $S(\omega)$  is the spectral field profile of the incident THz wave. If the Fourier filter is assumed a small hole, considerably smaller than the object size, located at a distance  $d$  from the optic center with an angle of  $\theta$ , or  $M(\xi,\eta) = \delta(\xi - d \cos \theta)\delta(\eta - d \sin \theta)$ , where  $\delta(\xi)$  is the Dirac delta function, Eq. (2) becomes

$$V(\omega; \theta) = C(\omega) \int_{\Sigma_o} dx dy U(x,y) e^{-ikd[f(x \cos \theta + y \sin \theta)]}. \quad (3)$$

Using the Fourier slice theorem [16], the projection of the image on the  $\theta$  direction, or sinogram, is obtained as

$$\tilde{S}(u, \theta) = \int_{\Sigma_o} dx dy U(x,y) \delta\left(x \cos \theta + y \sin \theta - \frac{fu}{d}\right), \quad (4)$$

which is the inverse Fourier transform of  $V(\omega, \theta)/C(\omega)$  with respect to  $\omega$ . Therefore, if we collect a sufficient number of measurements at different  $\theta$ s, the original object  $U(x,y)$  is then recovered using the inverse Radon transformation [16].

For the experiment, we used a Ti:sapphire laser oscillator which produced 50 fs short pulses at a repeti-

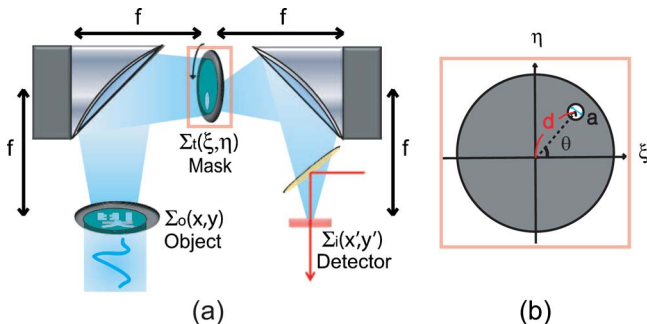


Fig. 2. (Color online) (a) Setup of THz single-point imagery and (b) mask geometry. The signal corresponds to the Fourier transform of the projection of the image.

tion rate of 100 MHz. The average power and the wavelength of the laser were 350 mW and  $\sim 800$  nm, respectively. For the generation and detection of THz waves, a large-area photoconductive antenna [17] and a 1-mm-thick ZnTe electro-optic crystal were used. The mask was fabricated with a 5 mm diameter hole, which was 15 mm off from the optic axis. A parabolic mirror with  $f=150$  mm was used as the transform optic  $L_t$ . The second parabolic mirror used as the imaging optic  $L_i$  had a short focal length of  $f'=100$  mm for a tight focus of the diffracted THz waves onto the detector, which was located at the center of the image plane,  $(x',y')=(0,0)$ . The time-domain signal of the THz wave was collected to retrieve the THz spectrum of up to 1.5 THz with a resolution of  $\sim 0.01$  THz.

Figure 3 illustrates the image recovery procedure. The test object used in the experiment is a Korean character meaning “light,” as shown in Fig. 3(a). The dimension of the nonopaque area of the object  $U(x,y)$  is  $2 \text{ cm} \times 2 \text{ cm}$ , being chosen to satisfy the field-of-view (FOV) condition (to be explained below). The entire area of the object is illuminated by collimated THz waves, and then  $N$  different waveforms uniformly sampled among  $\theta=0^\circ-180^\circ$  are collected. The 30 different temporal waveforms measured with  $\Delta\theta=6^\circ$  are presented in Fig. 3(b). The scan process needs to cover the first  $180^\circ$  of the angle, owing to the symmetry. Figure 3(c) shows the THz spectra

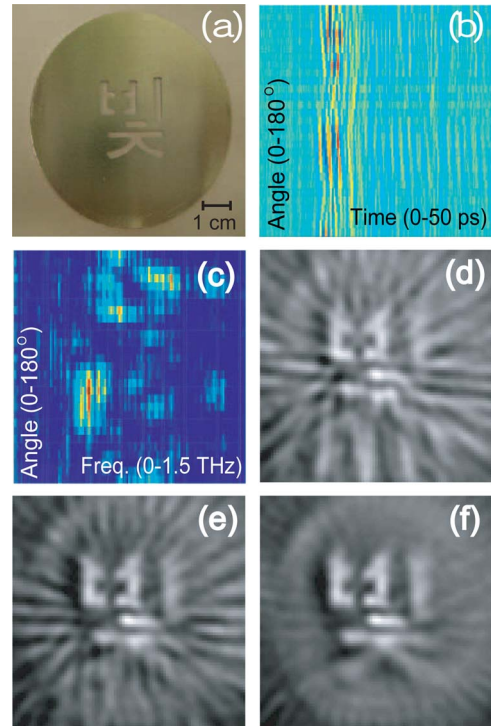


Fig. 3. (Color online) Image reconstruction process. (a) Target object  $U(x,y)$  with a Korean word meaning “light.” (b) Measured terahertz temporal profile  $V(t, \theta)$  presented as a function of the angle  $\theta$  of the mask. (c) Corresponding terahertz spectra  $V(\omega; \theta)$ . (d)–(f) Reconstructed images using inverse Radon transformation using (d) 10 waveforms measuring per  $18^\circ$ , (e) 15 waveforms measuring per  $12^\circ$  and (f) 30 waveforms per  $6^\circ$ , respectively.

$V(\omega; \theta)$ , which are Fourier transformed from the measurements in Fig. 3(b). The inverse Radon transformation of the sinogram data reconstructs the images in Figs. 3(d)–3(f). For the comparison of the recovered image qualities, 10, 15, and 30 waveforms among the measured  $N=30$  waveforms are selected for image reconstruction, respectively, in Figs. 3(d)–3(f). By using  $N=30$  waveforms, we were able to reconstruct images of reasonable quality.

As the hole in the mask had a finite diameter,  $a=5$  mm in the experiment, Eq. (3) needs correction owing to the Fraunhofer diffraction of a finite circular aperture [2]. Then  $U(x,y)$  in the integral calculation is replaced by

$$U'(x,y) = \pi a^2 U(x,y) \frac{2J_1(ka\rho/f)}{ka\rho f}, \quad (5)$$

where  $\rho = \sqrt{x^2 + y^2}$  and  $J_1$  is the first-order Bessel function of the first kind. This correction results in distortion to the reconstructed images, and the imaging FOV is limited as, for example,  $\rho_{\max} = 2.215fc/a\omega_{\max}$ , where  $\omega_{\max}$  is the THz cutoff frequency. By increasing the aperture size  $a$ , the signal  $V(\omega; \theta)$  increases by a factor of  $a^2$ , but the FOV decreases with  $1/a$ . Also, the FOV is considered inversely proportional to  $\omega_{\max}$ . Furthermore, the image resolution of our optical system is determined by the maximum spatial frequency, which is proportional to the distance to the hole,  $d$ . Simple calculation shows that the image resolution is given as  $\omega_{\max}d/fc$ . Hence, the larger  $d$  and the smaller  $a$  provide better image reconstruction at the expense of signal-to-noise ratio (SNR). On the other hand, the longer focal length  $f$  is good for FOV, although it is bad for image resolution. The imaging principle can be equivalently stated using time-of-flight (TOF) view point under geometric optics approximation and the assumption that the illuminated pulse is the delta function in time [18]. Note that at a specific time point, the scattered field from the equidistance TOF line arrives at the hole simultaneously. Hence, the measurement at the hole is the line integral along the TOF line.

The main disadvantage of the system is low SNR, since the hole mask blocks almost whole THz pulse. In the current setup, the signal strength, or the data acquisition efficiency, is sacrificed for the benefit of single-point imagery. For an efficient and better image quality, however, automatic repetition of pulse measurement using THz-AOS or powerful sources may make the SNR sufficiently large for real-time measurement. Also, an array of detectors on the spatial frequency plane can be used for parallel data acquisition, which further reduces the scanning acquisition time [11]. Furthermore, the digital spectral sampling on  $N$  different sets of THz frequency combs (frequency division multiple access) [19], or a set of different spectral waveforms (code division multiple

access) [20] in conjunction with THz waveform shaping [21] through  $N$  holes in the mask, may enable simultaneous measurements of  $N$  waveforms, allowing 2D image recovery from a single THz waveform.

In summary, we have demonstrated the single-point imagery of objects by exploiting the extreme broadband nature of ultrafast THz pulses. In this newly developed coherent optical computing scheme for a broadband source, 2D spatial information can be encrypted into waveforms, or a single waveform, and the image is recovered through inverse radon transformation. The THz imaging problem is now converted to 1D scanning rather than 2D one, which may significantly accelerate the acquisition time.

This work was supported in part by the IT R&D program of MKE/KEIT (2008-F-021-01), and in part by Basic Science Research Program through the National Research Foundation of Korea (2009-0083512).

## References

1. D. Casasent, *Computer* **12**, 27 (1979).
2. E. Hecht, *Optics*, 4th ed. (Addison Wesley, 2002).
3. B. I. Greene, J. F. Federici, D. R. Dykaar, R. R. Jones, and P. H. Bucksbaum, *Appl. Phys. Lett.* **59**, 893 (1991).
4. B. B. Hu and M. C. Nuss, *Opt. Lett.* **20**, 1716 (1995).
5. D. M. Mittleman, M. Gupta, R. Neelamani, R. G. Baraniuk, J. V. Rudd, and M. Koch, *Appl. Phys. B* **68**, 1085 (1999).
6. M. T. Reiten, D. Grischkowsky, and R. A. Cheville, *Appl. Phys. Lett.* **78**, 1146 (2001).
7. S. Wang, B. Ferguson, D. Abbott, and X. C. Zhang, *J. Biol. Phys.* **29**, 247 (2003).
8. W. L. Chan, K. Charan, D. Takhar, K. F. Kelly, R. G. Baraniuk, and D. M. Mittleman, *Appl. Phys. Lett.* **93**, 121105 (2008).
9. P. R. Smith, D. H. Auston, and M. C. Nuss, *IEEE J. Quantum Electron.* **24**, 255 (1988).
10. Q. Wu, T. D. Hewitt, and X.-C. Zhang, *Appl. Phys. Lett.* **69**, 1026 (1996).
11. B. Pradarutti, R. Muller, W. Freese, G. Matthäus, S. Riehemann, G. Notni, S. Nolte, and A. Tünnermann, *Opt. Express* **16**, 18443 (2008).
12. J. Xu and X.-C. Zhang, *Appl. Phys. Lett.* **88**, 151107 (2006).
13. D. L. Donoho, *IEEE Trans. Inf. Theory* **52**, 1289 (2006).
14. T. Yasui, E. Saneyoshi, and T. Araki, *Appl. Phys. Lett.* **87**, 061101 (2005).
15. D.-S. Yee, Y. Kim, and J. Ahn, in *Conference on Lasers and Electro-Optics* (Optical Society of America, 2009), paper JWA17.
16. O. K. Ersoy, *Diffraction, Fourier Optics and Imaging* (Wiley-Interscience, 2006).
17. A. Dreyhaupt, S. Winnerl, T. Dekorsy, and M. Helm, *Appl. Phys. Lett.* **86**, 121114 (2005).
18. K. H. Jin, Y. C. Kim, D. S. Yee, O. K. Lee, and J. C. Ye, *Opt. Lett.* **34**, 3863 (2009).
19. J. Olenewa and M. Ciampa, *Wireless Guide to Wireless Communications*, 2nd ed. (Course Technology, 2007).
20. V. Ipatov, *Spread Spectrum and CDMA* (Wiley, 2005).
21. J. Ahn, A. V. Efimov, R. D. Averitt, and A. J. Taylor, *Opt. Express* **11**, 2486 (2003).